ELSEVIER

Journal of Structural Geology 29 (2007) 1386–1399

JOURNAL OF STRUCTURAL GEOLOGY

www.elsevier.com/locate/jsg

Hydraulic connection and fluid overpressure in upper crustal rocks: Evidence from the geometry and spatial distribution of veins at Botrona quarry, southern Tuscany, Italy

Francesco Mazzarini*, Ilaria Isola

Istituto Nazionale di Geofisica e Vulcanologia, Sezione di Pisa, Via della Faggiola 32, 56100, Pisa, Italy

Received 21 June 2006; received in revised form 26 February 2007; accepted 27 February 2007
Available online 16 March 2007

Abstract

Veins are the geologic record of fluids that filled fractures at depth in the crust. In southern Tuscany (Italy), well-exposed Oligocene–Early Miocene sandstones hosting vein systems provide insight into the role of pore fluid and the stress state at the time of vein formation. The stress ratio ($\Phi = (\sigma_2 - \sigma_3)/(\sigma_1 - \sigma_3)$) and driving stress ratio ($R' = (P_f - \sigma_3)/(\sigma_1 - \sigma_3)$) were determined by analysing the distribution, length and aperture of fractures and veins and the magnitude of fluid overpressure. The derived fluid overpressure for the whole vein system ranges from 30 MPa to 64 MPa, with an average of 43 MPa; these values indicate that veins formed under supra-hydrostatic pressure conditions. Despite their spatial contiguity, two different vein arrays show very different stress and driving pressure ratios. One vein system is characterised by $\Phi = 0.62$ and $R' = 0.60$, the other by $\Phi = 0.54$ and $R' = 0.78$. The described vein systems are an example of a close spatial association of two non-hydraulically connected vein systems representing fluids focused through the upper crust.

Keywords: Fracture systems; Vein systems; Fluid overpressure; Sandstones; Tuscany

1. Introduction

Pore fluid pressure influences rock failure and the crack opening mode at depth in the crust, controlling the effective stress acting on a rock volume (Sibson, 2000 and references therein) and possibly triggering seismicity (Beeler et al., 2000; Miller et al., 2004). Fluids can saturate a rock volume or focus through fractures. Focused fluids in the crust are involved in metamorphic, magmatic and hydrothermal processes; they exploit the existing fracture network or generate new fractures. The connectivity and aperture of fractures provide a key for understanding the overall flow and transport properties of fracture networks (e.g. Darcel et al., 2003). Connectivity is important since not all the fractures in a rock volume can transport fluid, and connected fractures can create different hydraulic paths. Veins are defined as fractures that are mineralised at some depth in the crust, and can be used to study the geometric and hydraulic features of fracture networks in the crust (e.g. Vermilye and Scholz, 1995; Johnston and McCaffrey, 1996; Roberts et al., 1999). Veins are a record of fluid transport in fractures; when the fluid pressure builds up and then drops, minerals precipitate (Foxford et al., 2000; Bons, 2001; Cox et al., 2001). The geometric features and the spatial distribution of fractures and veins may thus be used to define parameters relating to fluid pressure, stress state and hydraulic connectivity between vein systems.

We report on the structural analysis of fracture networks and vein systems exposed in an abandoned sandstone quarry. The sandstones are well exposed in the quarry floors, allowing detailed mapping of fractures and veins at different depths (with a maximum step of about 10 m between floors). The calcite veins in the hosting sandstones formed in pre-existing fractures opened in pure extension and extensional shear

* Corresponding author. Tel.: +39 050 831 1956.
E-mail address: mazzarini@pi.ingv.it (F. Mazzarini).

0191-8141/$ - see front matter © 2007 Published by Elsevier Ltd.
doi:10.1016/j.jsg.2007.02.016

modes. Results are used to constrain the local fluid pressure, stress state and fracture connectivity in a fracture network that developed at very shallow crustal levels. We demonstrate that different non-hydraulically connected paths were in close spatial association at the time of vein formation.

2. Rationale

The type of failure affecting an intact rock mass greatly depends on the fluid pressure (P_f), since the effective principal stresses (Sibson, 2000 and references therein) are defined as:

$$\sigma'_1 = (\sigma_1 - P_f) > \sigma'_2 = (\sigma_2 - P_f) > \sigma'_3 = (\sigma_3 - P_f) \quad (1)$$

where σ_i ($i = 1,2,3$) are the principal stresses.

The ratio of pore fluid pressure to lithostatic pressure (σ_v) is defined as:

$$\lambda = P_f/\sigma_v = P_f/\rho g z \quad (2)$$

where ρ is the rock density and g is the gravitational acceleration.

Hydrostatic fluid pressure is attained when pores and fractures are interconnected up to the water table, which is assumed to reach the ground surface ($\lambda \sim 0.4$). Supra-hydrostatic fluid pressure conditions are defined by $0.4 < \lambda < 1.0$, while supra-lithostatic ones are defined by $\lambda > 1.0$ (Sibson, 2000).

Rock failure depends on the friction coefficient and on the equilibrium between differential stress ($\sigma_1 - \sigma_3$) and rock tensile strength T (Secor, 1965; Brace, 1978; Byerlee, 1978).

According to Sibson (2000), in the case of extension (i.e. $\sigma_1 = \sigma_v$) the pure extensional failure mode occurs when:

$$(\sigma_1 - \sigma_3) < 4T \quad (3a)$$

$$P_f - \sigma_3 = T \quad (4a)$$

and the extensional-shear failure mode occurs when:

$$4T < (\sigma_1 - \sigma_3) < 5.66T \quad (3b)$$

$$P_f - \sigma_3 = \left[8T(\sigma_1 - \sigma_3) - (\sigma_1 - \sigma_3)^2\right]/3 \quad \text{for } \mu_i = 0.75 \quad (4b)$$

where μ_i is the internal friction of the material.

Several parameters related to both the effective stress field and fluid pressure can be derived through the analysis of vein geometry, including vein attitude and aspect ratio (e.g., Baer et al., 1994; Jolly and Sanderson, 1997; Gudmundsson, 1999; André et al., 2001).

The stress ratio (Φ) and the driving stress ratio (R') are defined in terms of the principal stresses (σ_1, σ_2, σ_3) and fluid pressure (P_f) (Baer et al., 1994; Jolly and Sanderson, 1997):

$$\Phi = (\sigma_2 - \sigma_3)/(\sigma_1 - \sigma_3) \quad (5)$$

and

$$R' = (P_f - \sigma_3)/(\sigma_1 - \sigma_3) \quad (6)$$

The stress ratio Φ ranges from 0 to 1 and describes the Mohr circle configuration (Angelier, 1984; Baer et al., 1994; Orife and Lisle, 2003). The driving stress ratio R' (Baer et al., 1994) varies from -1 (no opening of fractures) to 1 (re-opening of pre-existing fractures), and describes the equilibrium between P_f and the minimum (σ_3) and maximum (σ_1) stresses.

The vein aspect ratio (W/L) is defined as the ratio between maximum vein aperture (W) and vein length (L). It can be used to derive static fluid overpressure (driving pressure) during vein formation, as it is assumed to be linearly related to fluid overpressure ($\Delta s_i = P_f - \sigma_3$) and the elastic properties of rocks (Gudmundsson, 1999 and references therein):

$$W/L = \Delta s_i 2(1 - \nu^2)/E \quad (7)$$

where ν and E are the Poisson ratio and Young's modulus, respectively.

Hydraulic and geometric features of veins and fractures such as length and aperture are characterised by scale invariance (e.g. Gillespie et al., 1999; Roberts et al., 1999; Bonnet et al., 2001; Bour et al., 2002; Darcel et al., 2003) and are analysed in terms of their cumulative frequency distribution and self-similar clustering.

The cumulative frequency distribution of the geometric features of fractures and veins (length, aperture) can be defined as:

$$N(>L) = \alpha L^a \quad (8)$$

where α is a normalisation constant, L is the fracture/vein length and a is the power law (fractal) exponent.

The spatial distribution (clustering) of fractures and veins is estimated through the computation of the respective correlation exponent D (e.g. Bonnet et al., 2001), which is a measure of how fractures (or veins) fill a space. In other words, two fracture networks with different correlation exponents exhibit different spatial distributions of fractures. The lower the D exponent, the higher the clustering of fractures. High D values indicate a homogeneous distribution of fractures. A homogenous distribution of fractures in trace maps yields $D = 2$. The two-point correlation method was used to measure the fractal dimension of the fracture/vein population. For a population of N points (fracture/vein barycentre) the correlation integral $C(l)$ is defined as the correlation sum that accounts for all the points at a distance of less than a given length l (Bonnet et al., 2001; Bour et al., 2002). In this approach, the term $C(l)$ is calculated as:

$$C(l) = 2N(l)/N(N-1) \quad (9)$$

where $N(l)$ is the number of pairs of points whose distance is less than l. If scaling holds, eq. (9) is valid, and the slope of the curve in a $\log(C(l))$ vs. $\log(l)$ diagram yields the D value.

Following eq. (9), the calculated D value is valid for a defined range of lengths (l). The distance interval over which eq. (9) is valid is defined by the size range. For each analysis, the size range of samples is in turn defined by a plateau in the local slope vs. $\log(l)$ diagram: the wider the range the better the calculation of the power law distribution (Walsh

and Watterson, 1993). The upper and lower cut-off values were defined according to the method described in Mazzarini (2004).

Truncation and censoring affect the calculated fractal distribution of fractures (e.g. Bonnet et al., 2001). In order to fit the data to a scale range probably not affected by these factors, about 200 fractures must be analysed in terms of their self-similar clustering using the fracture barycentre (Bonnet et al., 2001; Bour et al., 2002).

3. Geological outline

The studied quarry lies in the inner portion of the northern Apennine chain in southern Tuscany (Fig. 1). The chain is a Cenozoic fold-thrust belt resulting from the continental collision between the European margin and the Adria microplate (Boccaletti et al., 1971; Elter, 1975). It consists of northeastward thrusted allochthonous oceanic and continental nappes derived from the Alpine Tethyan Ocean (Ligurian domain) and the Adria plate (Tuscan and Umbro-Marchigian domains). The Ligurian Units crop out just east of the investigated area (Fig. 1). They consist of Cretaceous to Eocene argillites and calcareous-marly flysch sequences (Burgassi et al., 1983; Mazzarini et al., 2004; Musumeci et al., 2005). The Tuscan Nappe sedimentary sequence crops out extensively in the study area (Mazzarini et al., 2004; Musumeci et al., 2005). The sequence consists of Late Triassic–Jurassic platform and pelagic carbonate deposits, Late Jurassic pelagic siliceous sediments and finely laminated limestone, and Cretaceous to Oligocene red-green argillites with intercalated limestone. Late Oligocene–Early Miocene arenaceous flysch (Macigno Fm.; Cornamusini et al., 2002 and references therein) closes the sequence. The Neogene continental clastic deposits are Late Miocene conglomerates and Late Pliocene-Pleistocene conglomerates (Bossio et al., 1993; Musumeci et al., 2005). The magmatic rocks consist of granites of early Pliocene age (4.4 ± 0.6 Ma, Rb/Sr Wr-Bt; Serri et al., 2001; Mazzarini et al., 2004 and references therein) and are exposed a few kilometres east of the study area (Fig. 1).

The main structural feature in the area is the NNW–SSE trending fold system affecting the whole nappe stack (see Musumeci et al., 2005). In the area surrounding the Botrona quarry, the poles to bedding of Oligocene–Early Miocene sandstones distribute according to a gentle open fold (Fig. 2a) with a calculated axis plunging a few degrees to the NNW (340/1). This folding phase was coeval with the

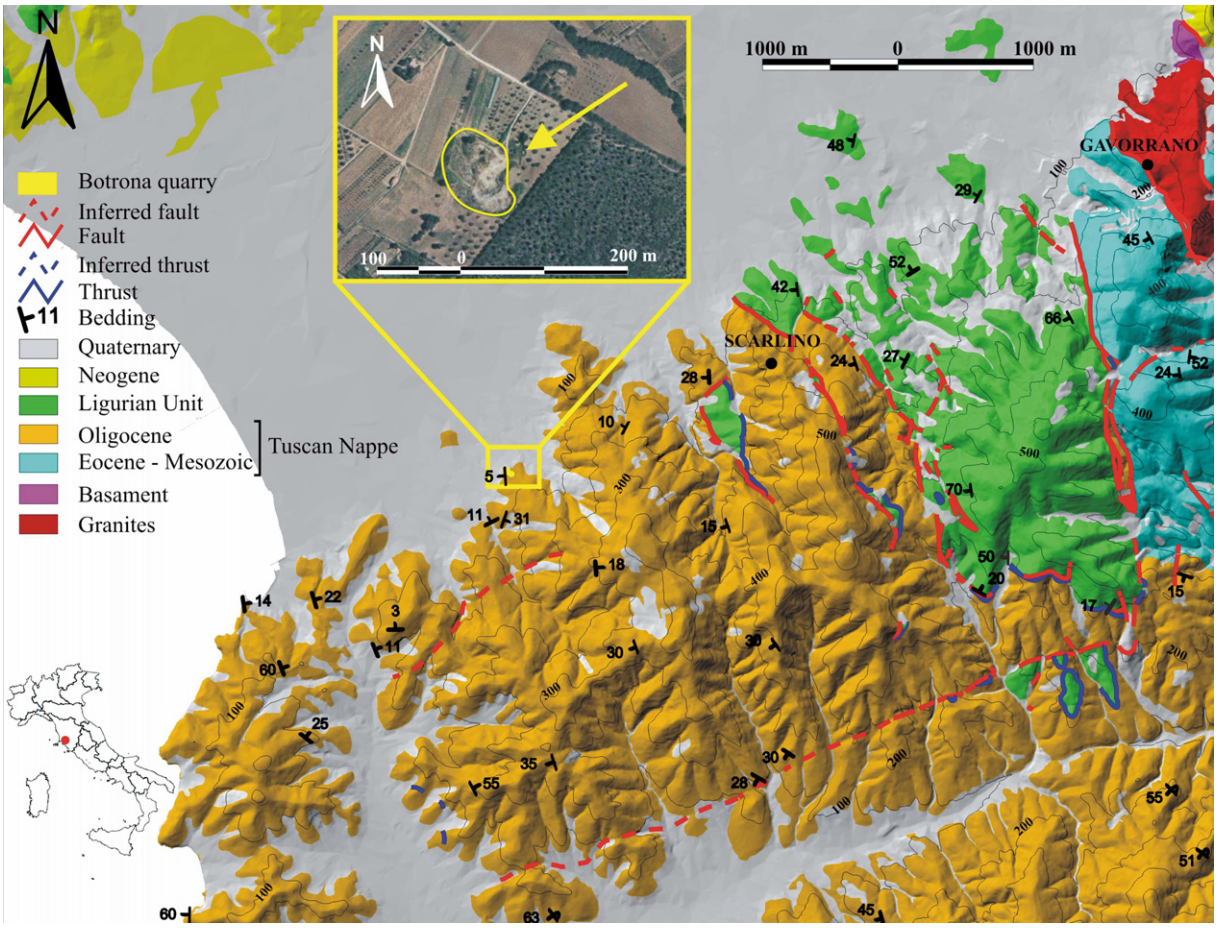

Fig. 1. Geological map of the quarry area. The Digital Elevation Model of the area is derived from the 10 m step DEM of Italy (Favalli and Pareschi, 2004). The geology of the area can also be downloaded from the Regione Toscana website (http://www.rete.toscana.it/sett/pta/terra/geologia /index.htm).

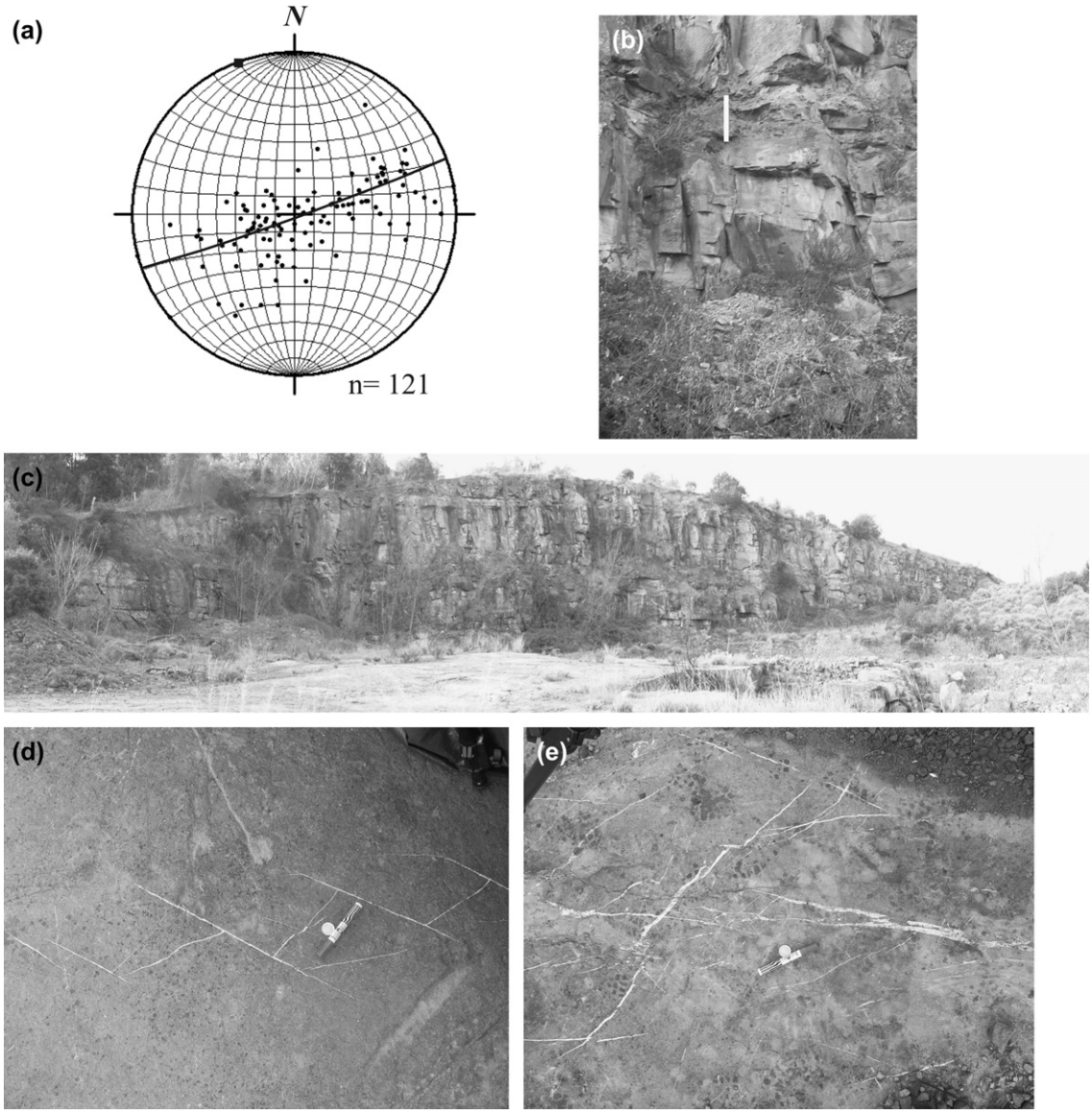

Fig. 2. (a) Lower hemisphere equal area stereonet showing poles to bedding from the Macigno sandstone. The interpolated axis (black square) of the gentle open fold is 340/1 (azimuth/plunge), number of planes = 121. (b) Thick beds of sandstones and the metre-thick intercalated siltitic layer (white line). (c) Quarry front, view from the east. (d) Organised vein arrays (OVA, see text for discussion); the pen is 13 cm long. (e) Distributed vein arrays (DV, see text for discussion); the pen is 13 cm long.

intrusion of the Pliocene granites, and was subsequently disrupted by the brittle tectonics which produced NNW–SSE normal and oblique high-angle faulting (Musumeci et al., 2005). Lastly, the development of E–W to ENE–WSW trending normal faults determined the general E–W trend of the main valleys (Bertini et al., 1969a,b).

In this context, the analysed fracture networks and vein systems may have developed either during the folding phase (e.g. Srivastava and Engelder, 1990) or during subsequent brittle extensional tectonics. Based on the generally steeply dipping attitude of fractures and of most veins, and on the occurrence of an E–W trending normal fault just a kilometre south of the quarry (Fig. 1), vein formation is thought to have occurred in a general extensional regime (i.e. $\sigma_1 = \sigma_v$).

3.1. Host rock

The rock hosting the vein systems consists of Oligocene–Early Miocene foredeep deposits belonging to the Macigno Formation (see Cornamusini et al., 2002). They are fine-grained turbidite sandstones with two massive beds about 3–4 m thick separated by fine-layered, 1 m-thick silty sandstones (Fig. 2b). The joints parallel to the bedding of the thick beds have a spacing of 0.62 ± 0.2 m. The sandstones in the quarry area are nearly horizontal or dip gently westward (average bedding attitude 265/5).

Although the elastic properties of the host rock are known to control crack formation (e.g. Gudmundsson, 1999), no direct measurements of the elastic properties of the studied

Macigno Formation sandstones are available. In the literature (e.g.: Jaeger and Cook, 1969; Goodman, 1980; Turcotte and Schubert, 2002; Gerecek, 2007) and the web (http://www.liv.ac.uk/seismic/links/info.html). Young's modulus for sandstones varies from 10 to 25 GPa and the Poisson ratio ranges from 0.21 to 0.38. The sandstone tensile strength is estimated to be 5–25 MPa, while the bulk density is assumed to vary in the 2000–2500 kg m^{-3} range.

In the study area, the sandstones of the Macigno Formation are covered by the Ligurian Units and by Miocene–Pliocene deposits (e.g. Mazzarini et al., 2004; Musumeci et al., 2005). Considering a Pleistocene uplift of about 650 m in southern Tuscany (Marinelli et al., 1993), a maximum thickness of eroded overlying units of about 3-4 km is estimated for the sandstones at the time of the development of the analysed vein systems.

4. Fracture network and vein systems

The Botrona quarry is 50 m a.s.l. and located just a few kilometres from the coast near the village of Scarlino, in southern Tuscany (Fig. 1). The quarry covers an area of about 7000 m^2; the quarry front is up to 13 m high and extends for 80 m in an E–W direction (Fig. 2c). Two main horizons were quarried, with the exposed levels showing a 10 m difference in elevation (Fig. 3). The two floors in the quarry are labelled L1 (the upper one) and L2 (the lower one). In order to describe the fracture network and the attitude of vein systems, the aperture and length of fractures and veins were measured, and fracture and vein trace maps were compiled. Photo mosaics (samples) of the quarry floor were created for different sites; sampling site locations are shown in Fig. 3. The length of fractures, and the length and aperture of veins were thus sampled (Fig. 4). Four samples come from the upper quarry level (L1), and three from the lower level (L2). The fracture density (fractures and veins) in quarry floors was determined by counting the number of intersecting fractures along randomly directed 1 m-long scan lines. The fracture density in the quarry as a whole is 11.2 ± 5.1 m^{-1}. Fracture density is 13.1 ± 5.8 m^{-1} in the L1 floor and 9.1 ± 3.2 m^{-1} in the L2 floor.

The fracture (vein) density in the sampled sites was also estimated by analysing the compiled fracture trace maps (Fig. 4). The fracture (vein) density (m^{-1}) in each of the sampled sites was computed as the ratio between the cumulative length of fractures (veins) and the sampled area. The fracture density

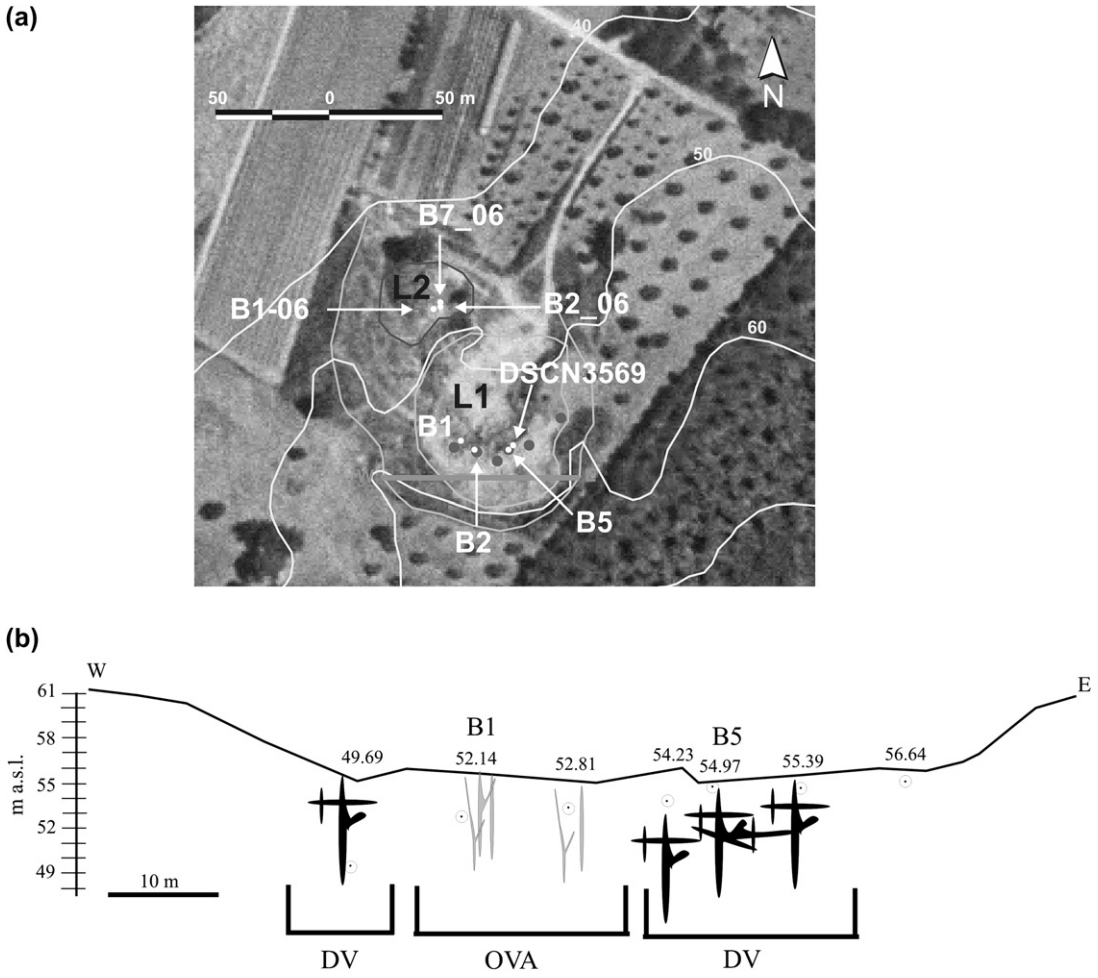

Fig. 3. (a) Locations of the sampled sites in the Botrona quarry. L1 and L2 are the two exposed quarry pavements. The light gray solid line is the trace of the profile in point b. (b) E–W profile onto which points (white dots) are projected with their elevations. Black pattern: Distributed Veins array (DV); light gray pattern: Organised Vein Array (OVA).

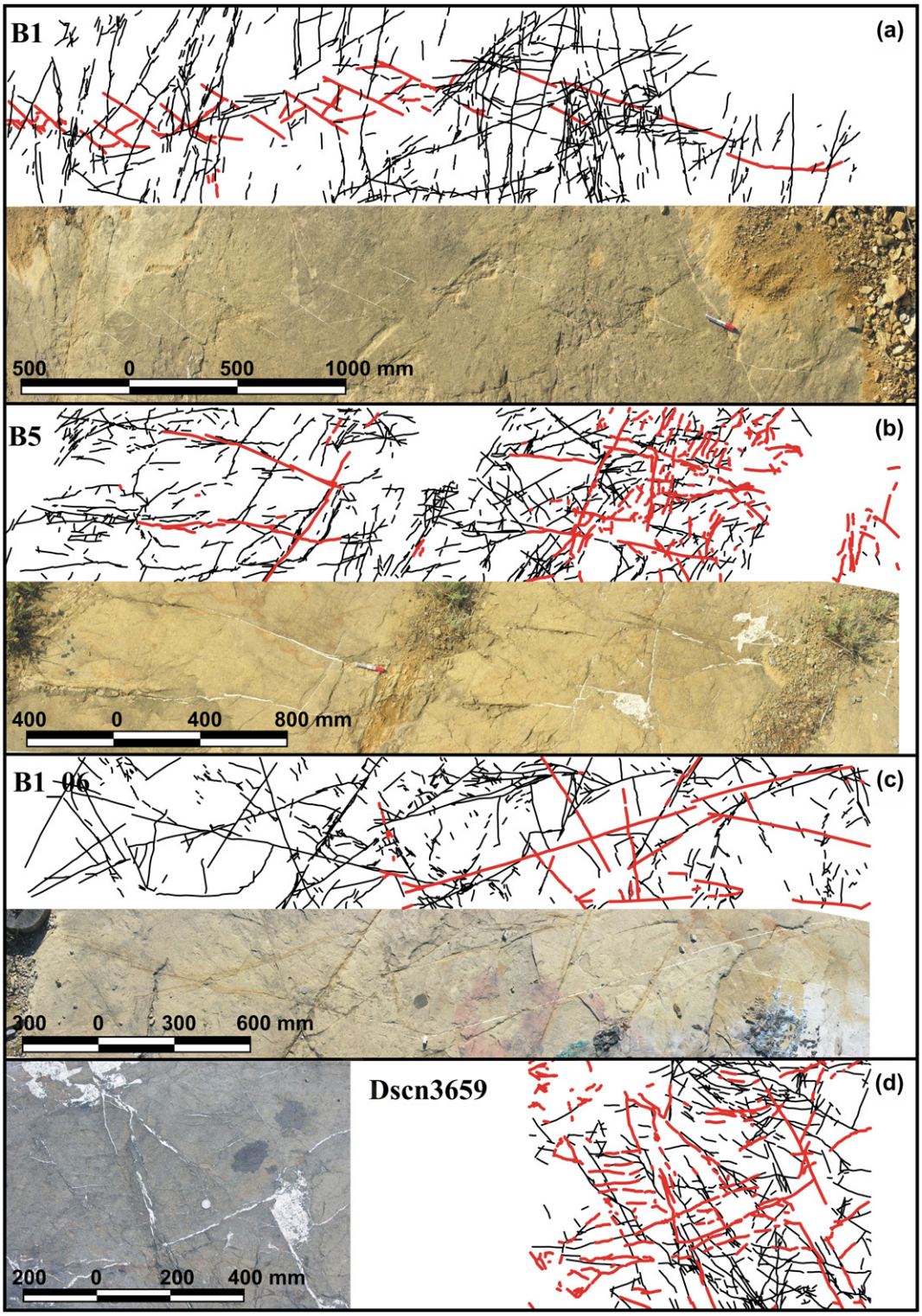

Fig. 4. Trace maps of fractures and veins in four selected samples (see Fig. 3 for locations). (a) Trace maps and photo mosaic of B1. (b) Trace maps and photo mosaic of B5. (c) Trace maps and photo mosaic of B1_06. (d) Trace maps and photo mosaic of DSCN3569.

averaged over all the samples is 15.4 m^{-1}. The fracture density is 18.1 m^{-1} in the upper level of the quarry (L1) and decreases to 11.7 m^{-1} about 10 m below (level L2). The average vein density is 6.9 m^{-1}. Vein density is 6.6 m^{-1} in level L1 and 7.4 m^{-1} in L2.

4.1. Fracture network

Observed fractures in the Botrona quarry cluster into five main trends: E–W, NE–SW, NW–SE, NNW–SSE and N–S (Fig. 5a). Fractures are generally steeply dipping or vertical

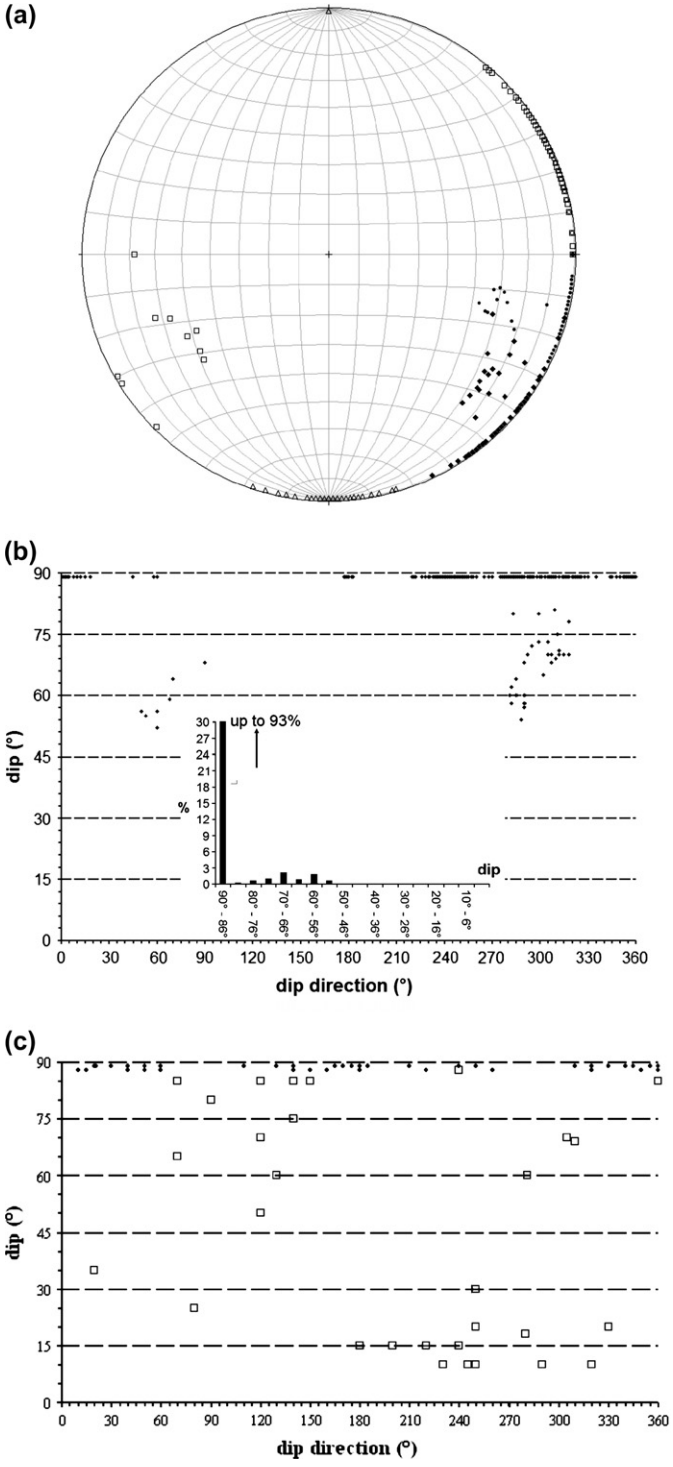

Fig. 5. (a) Lower hemisphere equal area stereonet showing poles to fractures ($n = 455$). Black dots: N–S trend; open circles: NNW–SSE trend; open triangles: E–W trend; open boxes: NW–SE trend; black diamonds: NE–SW trend. (b) Plot of fracture strike vs. fracture dip. (c) Plot of vein strike vs. vein dip; vein in OVA black diamonds, vein in DV open squares.

(Fig. 5b). Most of the fractures show no apparent evidence of shear and appear to be generally mode I fractures. Moreover, they show no systematic abutting relationships and locally show mutual cross-cutting relationships that indicate coeval formation.

Fracture length varies from 5.6 m down to 3×10^{-2} m, with an average value of 0.39 m. The coefficient of variation C_V describes the distribution of fracture lengths: $C_V > 1$ indicates clustering, $C_V = 1$ indicates a random or Poisson distribution, and $C_V < 1$ indicates anti-clustering (homogeneous distribution) of fracture length (Gillespie et al., 1999 and references therein). C_V is defined as:

$$C_V = s/m \tag{10}$$

where s is the standard deviation and m is the mean.

The observed fracture network has a clustered length distribution with $C_V = 1.376$.

The spacing of the fracture systems was also analysed: it varies from a maximum of 1.36 m to a minimum of 10^{-2} m, with an average of 9.9×10^{-2} m. It is clustered with $C_V = 1.273$.

In eq. (8), the measured fracture lengths show a power law distribution. In the $\log(l)$ vs. $\log(N(>l))$ space (Fig. 6a) the curve shows two trends: one for fractures less than 0.33 m long ($(N(>L)) = 2068.7 \times L^{-0.7149}$, $R^2 = 0.9952$), the other for fractures 0.33–2.4 m long ($(N(>L)) = 46715 \times L^{-1.5803}$, $R^2 = 0.9971$). The distribution is mainly controlled by long fractures when $a < 1$, whereas it is controlled by shorter fractures when $a > 1$ (e.g. de Dreuzy et al., 2004).

Fracture network connectivity controls the occurrence and distribution of hydraulic paths, and is in turn controlled by the spatial clustering of fractures (e.g. Bour et al., 2002; de Dreuzy et al., 2004). The correlation exponent (D) was calculated for the fracture trace maps of the samples with more than 200 traces (eq. (9) and Table 1). In the quarry $D = 1.63 \pm 0.07$ in the 0.004–0.45 m length range, in the L1 level $D = 1.67 \pm 0.01$ in the 0.004–0.44 m length range, and in the L2 level $D = 1.56 \pm 0.02$ in the 0.004–0.46 m range (Fig. 7a). The correlation coefficient of the fracture network is well defined in all levels of the quarry, and fractures in level L2 are more clustered than those in L1.

4.2. Vein systems

The veins are unevenly distributed on the quarry floors and tend to cluster in zones 5–10 m apart. They may occur in NE–SW trending belts about 2 m wide or in broad zones about 7 m wide with no particular trend (Fig. 2d,e). Vein infilling consists of euhedral calcite crystals.

The veins in the belts are arranged in segmented systems several decimetres long. The systems consist of veins, each with a variable aperture of one to several millimetres and vertical to sub-vertical dip, that define NE–SW and E–W oriented vein arrays (Fig. 5c). We defined these vein belts as organised vein arrays (OVA; Fig. 2d).

The veins in the broad zone have a dispersed pattern, with variable dip angles and apertures of one millimetre to a few centimetres. They are sinuous veins that frequently show hook and branching geometries. The azimuth distribution of these veins is dispersed, and their dip angle may be very low (less than 10°); NE–SW and E–W trends are also present

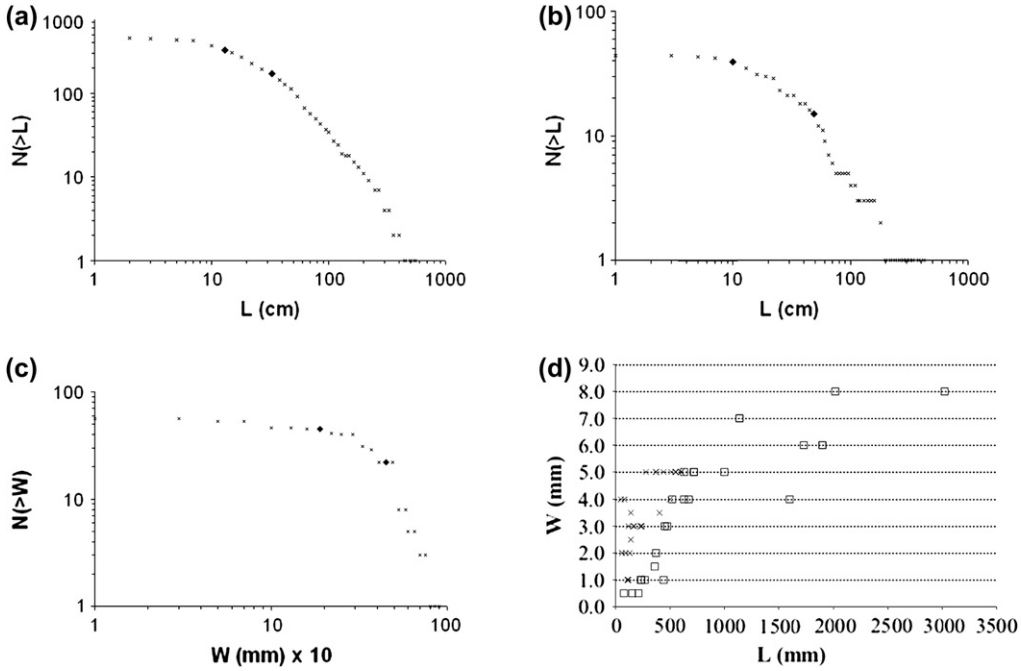

Fig. 6. (a) Cumulative distribution of fracture length, plot of $N(>L)$ vs. L. (b) Cumulative distribution of vein length, plot of $N(>L)$ vs. L. (c) Cumulative distribution of vein width, plot of $N(>W)$ vs. W. (d) Plot of W vs. L for veins; open squares represent unconstrained veins.

and are characterised by horizontal diversion along the bedding plane (Figs. 5c and 8g). The veins in the broad zones are defined as distributed veins (DV; Fig. 2e).

Field observations point to different fluid pressures in the two systems. In the L1 floor, the elevation of the OVA is 1–2 m lower than that of the DV system (Fig. 3). Moreover, OVA shows lateral expansion (i.e. horizontal diversion; see Fig. 8g) of veins 5 m upward, i.e. 3 m above the DV system. If the two spatially close vein systems had been hydraulically connected, the level of lateral vein expansion would have been the same for the two systems.

Veins in the OVA exploit fractures (Fig. 8a–c): the observed vein length to fracture length ratio is 0.89 ± 0.07. OVA veins are generally pure extensional veins, with the opening vector normal to the vein walls and marked by the growth of calcite crystals. In some cases veins cut fractures, and the separation between the two fracture segments is parallel to the opening direction of the vein (Fig. 8b). There are also examples of extensional veins with minor left lateral shear with dilatant jogs developed on stepovers on parallel fractures (Fig. 8c). In contrast, DV comprise fractures exploited by veins as well as newly formed veins. DV veins are pure extension veins and extensional shear veins (Fig. 8d–f).

Comparison of vein segment morphology in both OVA and DV systems with experimentally produced fracture systems (Pollard et al., 1982; Nicholson and Pollard, 1985) shows that the formation and propagation of vein segments such as those in OVA is mainly controlled by far-field stress (i.e. tectonic stress), whereas the DV-like vein segments appear mainly controlled by near-field stress created by the forceful emplacement of fluids, as also indicated by the occurrence of host rock chips and blocky calcite in the studied DV veins (Fig. 8h).

The length (L), aperture (W) and spacing (S) of vertical veins in the E–W and NE–SW vein systems of the OVA were

Table 1
Correlation exponents of fractures in the sampled sites

Sample	Vein system	Level	n	L. cut-off (m)	U. cut-off (m)	D	c	R^2
B1	OVA	L1	1014	0.005	0.48	1.68	2×10^{-5}	0.999
B5	DV	L1	1069	0.005	0.48	1.66	1×10^{-5}	0.999
Dscn3659	DV	L1	501	0.002	0.36	1.68	5×10^{-5}	0.999
B1_06	OVA	L2	202	0.004	0.44	1.57	5×10^{-5}	0.999
B2_06	OVA	L2	772	0.004	0.48	1.54	4×10^{-5}	0.999
Summary								
Total				0.004 ± 0.001	0.45 ± 0.05	1.63 ± 0.07	$(3.4 \pm 1.8) \times 10^{-5}$	0.999
L1				0.004 ± 0.002	0.44 ± 0.07	1.67 ± 0.01	$(2.7 \pm 2.1) \times 10^{-5}$	0.999
L2				0.004 ± 0.001	0.46 ± 0.07	1.56 ± 0.02	$(4.5 \pm 0.02) \times 10^{-5}$	0.999

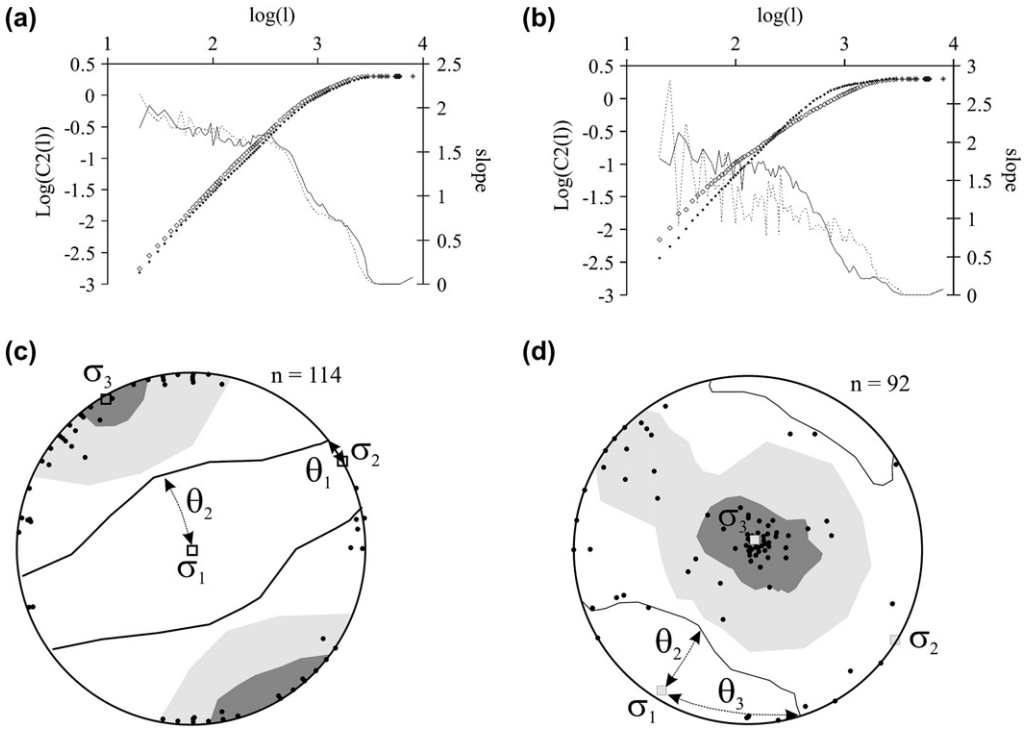

Fig. 7. (a) Plot of log(C2(l)) vs. log(l) for fractures; B1: open diamonds; B5: small black diamonds. (b) Plot of log(C2(l)) vs. log(l) for veins; B1: open diamonds; B5: small black diamonds. (c) Lower hemisphere equal area stereonet showing poles to veins ($n = 114$) for OVA vein systems. Dark grey > 5%; light grey > 3%; white > 1%. $\sigma_1 = 204/89$; $\sigma_2 = 60/1$; $\sigma_3 = 330/1$. Angles θ_1 (9°) and θ_2 (39°) define the vein distribution according to Jolly and Sanderson (1997). (d) Lower hemisphere equal area stereonet showing poles to veins ($n = 92$) for DV. Dark grey > 5%; light grey > 3%; white > 1%. $\sigma_1 = 212/6$; $\sigma_2 = 122/2$; $\sigma_3 = 17/84$. Angles θ_2 (28°) and $\theta 3$ (44°) define the vein distribution according to Jolly and Sanderson (1997).

systematically measured. The statistics and C_V coefficients for the geometric features of veins are listed in Table 2. The overall vein length shows a nearly random or Poisson distribution ($C_V = 0.955$); the NE–SW system shows a clustered length distribution ($C_V = 1.195$), while the E–W system shows the most regular length distribution ($C_V = 0.605$). The spacing of the vein systems varies from a minimum of 10^{-2} m to a maximum of 0.28 m, with an average of 0.13 m; spacing is not clustered ($C_V = 0.710$; Table 2). The NE–SW system has an average spacing of 0.12 m ($C_V = 0.724$), and the E–W system an average spacing of 0.10 m ($C_V = 0.674$). The average vein width is 0.35 cm, and widths are almost regularly distributed ($C_V = 0.494$). The average aperture of the NE–SW system is 0.31 cm ($C_V = 0.776$), while that of the E–W system is 0.35 cm ($C_V = 0.355$).

The measured vein lengths show a power law distribution. In the log(l) vs. log($N(>l)$) plot (Fig. 6b), the curve shows two trends: one for veins 0.01–0.49 m long ($N(>L)) = 172.01 \times L^{-0.6153}$, $R^2 = 0.9701$), the other for veins 0.5–1.8 m long ($N(>L)) = 1551.7 \times L^{-1.2769}$, $R^2 = 0.9171$).

In the log(W) vs. log($N(>W)$) plot, the measured vein thicknesses (W) show a rough power law distribution (Fig. 6c) for $W < 4.5$ mm ($N(>W)) = 568.71 \times W^{-0.8366}$, $R^2 = 0.8489$). The curve is very steep for $W > 4.5$ mm ($N(>W)) = 7 \times 10^8 \times W^{-4.5481}$, $R^2 = 0.9333$), probably due to undersampling of thicker veins (censoring effect; Bonnet et al., 2001).

The aperture to length ratio (W/L) was determined for veins that met the following criteria (see Gudmundsson, 1999): (1) mode I fractures with no appreciable shear displacement; (2) veins that did not intersect other fractures or rock discontinuities (non-restricted veins). Their length was defined as the linear distance from the ends of a continuous mineral-filled fracture. Only 41 veins in the whole quarry met the criteria listed above; they have an average W/L ratio of 0.005 (±0.002), a minimum ratio of 0.001 and a maximum ratio of 0.008. DV mainly scatter in the left portion of the W vs. L plot (Fig. 6d).

As in the case of fractures, the correlation exponent (D) was calculated using the trace maps of veins in the sampled sites in order to evaluate the spatial clustering of veins. In the case of vein trace maps, only samples with at least 90–100 traces were analysed (four samples; Table 3). The reduced number of veins may introduce bias in the estimation of cut-off values due to censoring and truncation effects (e.g. Bonnet et al., 2001). The bias introduced in the OVA data (relatively low number of veins, 96, Table 3) is always lower than the difference between the correlation exponent of OVA and DV systems. The OVA veins in level L1 have a D value of 1.18 ± 0.02 in the 0.08–0.4 m length range, whereas the DV (always in level L1) have $D = 1.64 \pm 0.02$ in the 0.05–0.4 m length range (Fig. 7b). Only OVA veins were measured in the lower level (L2), where $D = 1.38 \pm 0.02$ in the 0.02–0.6 m range.

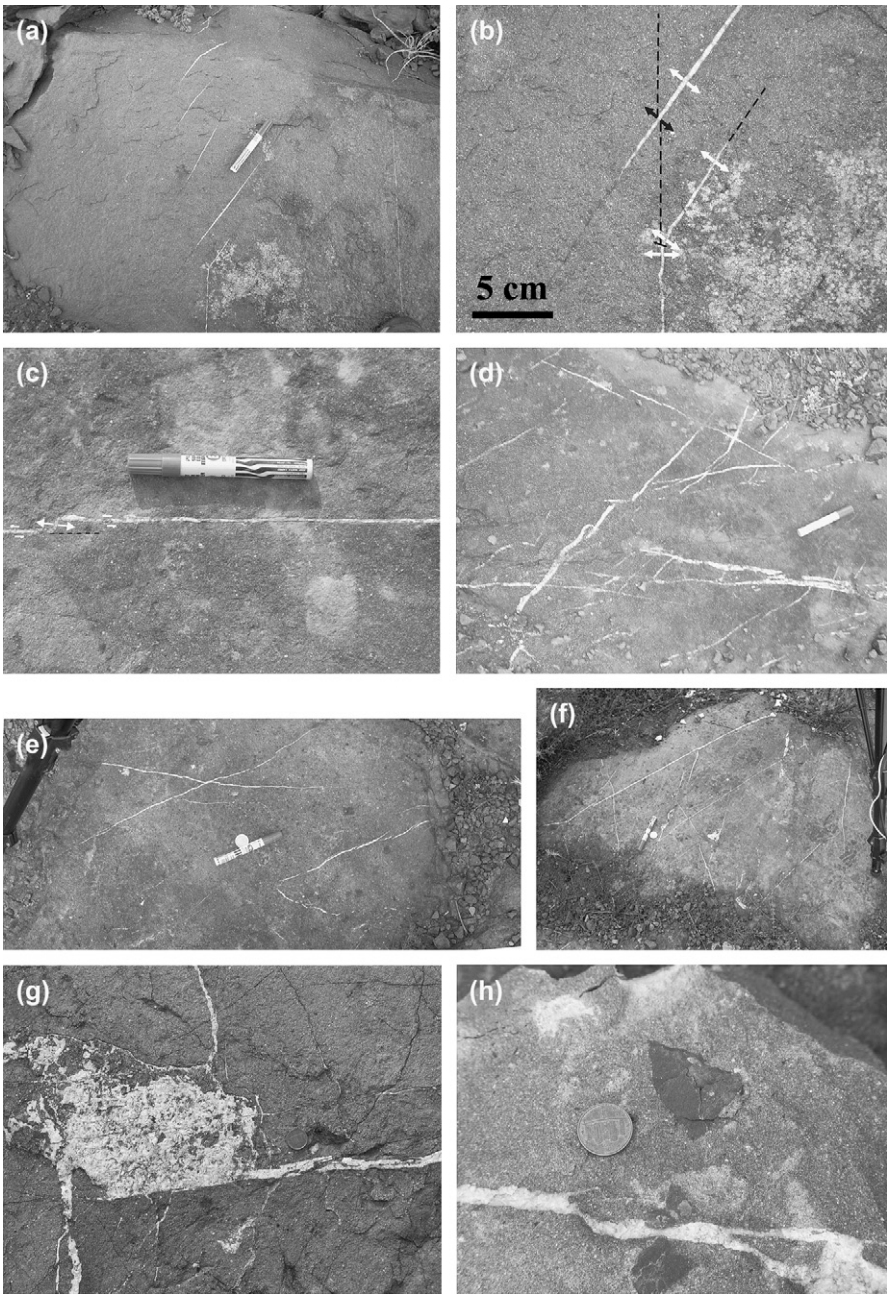

Fig. 8. (a) NE–SW and E–W veins in OVA system; pen is 13 cm long and points to the east. (b) Close up of (a); black dashed line marks the fracture traces, white arrows mark the opening direction of calcite veins, black arrow marks the offset of the NE–SW fracture, small black arrow is the direction of the vein deflection. (c) Two NE–SW vein segments in the OVA system linked by a dilatant jog on stepovers between fractures (black dashed line: fracture; white arrows: opening directions and sense of shear); the veins have minor left later shear. The thicknesses of veins and of dilatant jog are quite similar and the jog is nearly normal to the vein traces; pen is 13 cm long. (d–f) NE–SW and NNW–SSE extensional shear veins in DV system; the pen is 13 cm long and points to the north. (g) NE–SW veins feeding sub-horizontal vein; coin diameter is 1.6 cm. (h) Host rock chips in NNW–SSE vein in DV system; the coin diameter is 2 cm.

5. Fluid overpressure, driving pressure ratio and stress ratio

The different patterns and geometries of veins in the Botrona quarry can be used to constrain the stress field and fluid pressure state at the time of their formation. In particular, assuming that veins in the Botrona quarry are unconstrained and formed in a homogenous medium (e.g. Gudmundsson, 1999), it is possible to derive the fluid overpressure Δs_i ($P_f - \sigma_3$) using eq. (7) and the observed W/L ratio of 0.005. The result greatly depends on the elastic properties of sandstones, in particular on the Young's modulus. In the case of the Botrona quarry, the derived fluid overpressure Δs_i ranges from 30 MPa to 64 MPa, with an average value of 43 MPa.

Such a high fluid overpressure suggests that veins in the Botrona quarry formed under supra-hydrostatic conditions

Table 2
Statistics of length, aperture and spacing of veins systems

Data set	n	Average L (cm)	Max. L (cm)	Min. L (cm)	L C_V	Average W (cm)	Max. W (cm)	Min. W (cm)	W C_V	Average S (cm)	Max. S (cm)	Min. S (cm)	S C_V
E–W	29	36.4	100	6	0.605	0.35	0.8	<0.1	0.355	10.0	28	1	0.724
NE–SW	17	52.6	190	5	1.195	0.31	0.7	<0.1	0.776	12.5	25	7	0.674
Total	46	47.4	190	5	0.955	0.35	0.7	<0.1	0.494	10.3	28	1	0.710

L, vein length; S, vein spacing; W, vein aperture; C_V, coefficient of variation.

with $0.4 < \lambda < 0.8$. Assuming an extensional setting, the general equation for the maximum depth of vein formation (e.g. Suppe, 1985) can be applied:

$$h \approx \mathrm{abs}[nT/\rho g(1-\lambda)] \tag{11}$$

where h is the maximum depth of vein formation, T is the rock tensile strength, ρ is the rock density, n is 3 for a mode I aperture and 4.83 for a mixed mode aperture, and g is the acceleration of gravity. For the Macigno sandstones, we assume T in the range of 5–10 MPa and a bulk rock density of about 2500 kg m^{-3}. The derived maximum vein depth ranges from ~1 to ~7 km, with an average of ~3 km.

In the L1 quarry floor, two vein arrays are a few metres apart (Fig. 3): one array represents the OVA type (sample B1 in Fig. 3) and the other the DV type (sample B5 in Fig. 3). The orientation of the principal stress axes is derived from the vein distribution calculating the Bingham distribution (e.g. Press et al., 1986) of vein poles, and assigning each eigenvector to the appropriate principal stress. At the Botrona quarry there are pure extension and extensional shear veins (Figs. 4 and 8). We assume that the largest eigenvector is the smallest principal stress (σ_3) for both OVA and DV vein systems. The lack of sub-horizontal veins in the OVA system (Fig. 7c), a feature not due to sampling bias, implies that the maximum principal stress (σ_1) is vertical. Conjugate extensional shear veins are frequent in the DV system (Fig. 8d–f) and are compatible with σ_1 oriented nearly NE–SW (212/6). Based on these observations the smaller eigenvector is identified as the maximum principal stress.

Plots of pole to veins for samples B1 (OVA) and B5 (DV) thus show two quite different vein distributions described by three angles: θ_1, θ_2 and θ_3 (Fig. 7d,e). θ_1 is the angle between the σ_2 stress axis and the border of vein distribution in the σ_2–σ_3 plane; θ_2 is the angle between the σ_1 stress axis and the border of vein distribution in the σ_1–σ_3 plane, and θ_3 is the angle between the σ_1 stress axis and the border of vein distribution in the σ_1–σ_2 plane (Jolly and Sanderson, 1997). The attitude distribution of veins may thus be used to infer the stress ratio (5) and the driving pressure ratio (6). According to Jolly and Sanderson (1997), the stress ratio for the aperture of a pre-existing fracture can be derived from angles θ_1, θ_2 and θ_3:

$$\Phi = (1+\cos 2\theta_2)/(1+\cos 2\theta_1), \;\; P_f < \sigma_2 \tag{12}$$

and

$$\Phi = 1 - [(1-\cos 2\theta_2)/1-\cos 2\theta_3)], \;\; P_f > \sigma_2 \tag{13}$$

The driving pressure ratio is defined as:

$$R' = (1+\cos 2\theta_2)/2 \tag{14}$$

Applying these equations to samples B1 and B5, the Φ and R' values are derived for both types of vein arrays. The OVA (sample B1) is characterised by $\Phi = 0.62$ and $R' = 0.60$, whereas the DV array (sample B5) is characterised by $\Phi = 0.54$ and $R' = 0.78$.

6. Conclusions

The vein systems in the Botrona quarry developed at shallow crustal levels by exploiting the present fracture network. Based on the vein geometry, fluid overpressure was estimated to range from 30 to 64 MPa (average 43 MPa). Based on geological observations, the maximum depth of sandstones at the time of vein formation is assumed to have been 3–4 km. The fracture formation depth of ~3 km estimated through eq. (11) agrees with geological observations. At this depth, hydrostatic fluid pressure ranges from 29 to 39 MPa; the average fluid overpressure of 43 MPa indicates a supra-hydrostatic ($\lambda > 0.4$) pressure fluid at the time of vein formation. The two main vein arrays in the quarry differ in pattern and distribution. They have been defined as OVA and DV arrays (Fig. 2d,e). Considering the calculated stress ratio (Φ) and driving pressure ratio (R') for the two vein systems (OVA and DV, Fig. 7d,e), fluid pressure is greater than intermediate stress for the DV, whereas it is lower than intermediate stress for the OVA. This difference is not determined by the existing fracture networks in the two sites. The spatial distribution of fractures in the two sites (OVA and DV) is quite similar, as the correlation

Table 3
Correlation exponents of veins in the sampled sites

Sample	Vein system	Level	n	L. cut-off (m)	U. cut-off (m)	D	c	R^2
B1	OVA	L1	96	0.08	0.40	1.18	4×10^{-4}	0.999
B5	DV	L1	327	0.05	0.40	1.67	3×10^{-5}	0.999
Dscn3659	DV	L1	297	0.02	0.40	1.60	7×10^{-5}	0.999
B1_06	OVA	L2	215	0.02	0.60	1.38	1×10^{-4}	0.999

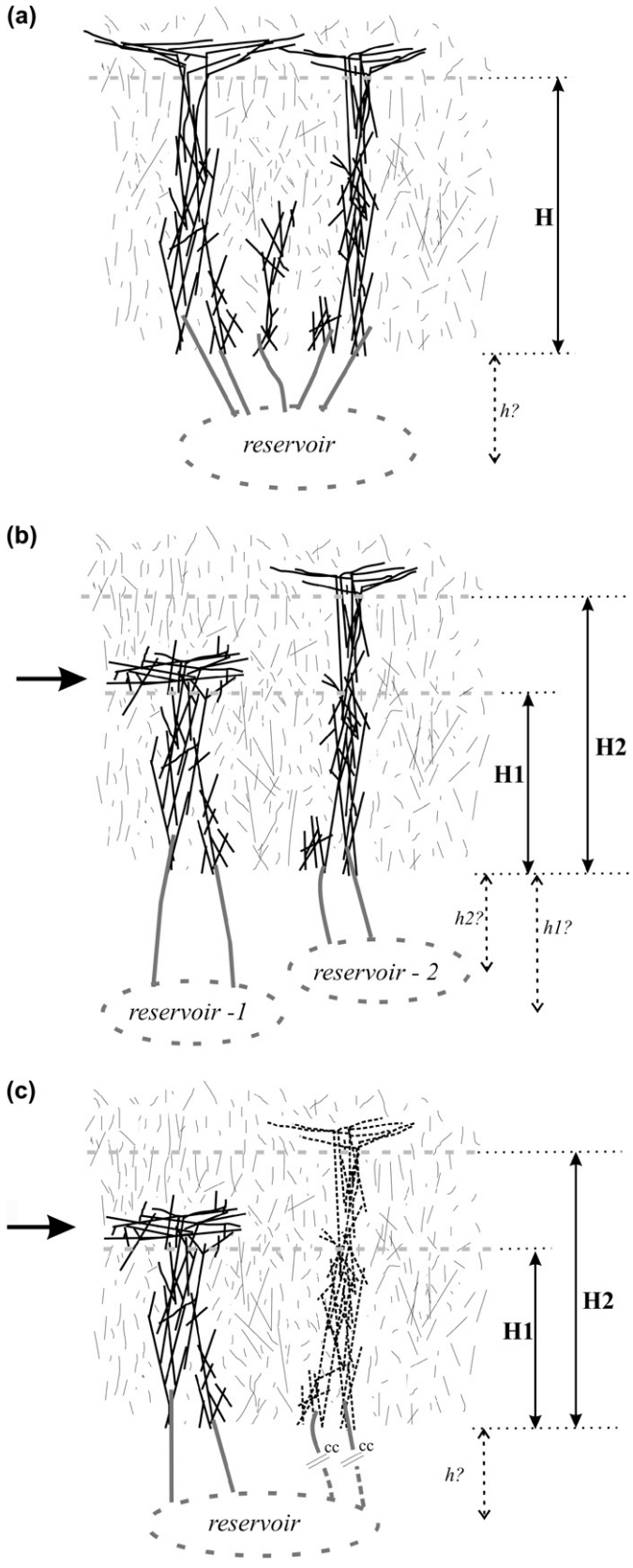

Fig. 9. Conceptual models on the formation of hydraulically not connected veins systems in close spatial association as OVA and DV veins. Thin black lines are fractures. Thick black lines are the connect portions of the fracture network (connected paths). Grey thick lines represent the link between the fluid reservoir and the analysed connected paths. Dashed horizontal grey lines are the levels where horizontal diversion of the connected paths occur. (a) Focused flows in a fractured volume of rock, the fluid exploits the connected paths in the fracture network; all paths share the same fluid pressure. H is the level at which the paths have horizontal diversion; h is the depth of the hypothetical fluid reservoir (see text). (b) Different reservoirs feed different connected paths. H1 is the level of horizontal diversion for the hydraulic path connected with the deepest (h1) fluid reservoir. H2 is the level of horizontal diversion for the hydraulic path connected with the shallowest (h2) fluid reservoir. The fluid pressure in the H1 path is higher than fluid pressure in the H2 path. Black arrow: actual level of exposure at Botrona quarry. (c) At depth h one fluid reservoir feeds all the connected paths as in point (a). At some time the connection between the reservoir and the principal path closes (cc) and this path is sealed (thick dashed black lines). The fluid pressure increases in the other path; it has horizontal diversion at a level H1 lower than H2. Black arrow: actual level of exposure at Botrona quarry.

exponent (D) testifies (Fig. 7a and Table 1); however, the two systems show quite different vein clustering (Fig. 7b and Table 3), the DV veins being less clustered than the OVA veins.

The attitude of OVA veins indicates that they formed in an extensional regime (i.e. $\sigma_1 = \sigma_v$). The OVA system is coherent with a stress field characterised by NW–SE (330/1) extension consistent with ENE–WSW normal faulting in the area. The minimum principal stress of the DV system is vertical and is supposed to be controlled by the local influence of fluid pressure that produced a horizontal diversion of veins and inflation of the overburden. Veins exploited inherited sub-horizontal discontinuities such as bedding planes and/or parallel joints.

The OVA and DV vein systems are few meters apart in a fractured medium, and the vein infilling is similar in composition (calcite). Fluid circulation in the two vein systems was probably similar, and occurred through focused paths representing the connected portion of the fracture network. CO_2-rich fluids may have derived from fluid circulation at depth, where carbonate formations are present in the nappe stack. Moreover, important carbon-dioxide fluxes from mantle degassing are documented in central Italy (Chiodini et al., 2000, 2004). Fluid inclusion analysis as well as microstructural studies on vein fabric are in progress since they are essential for fully understanding fluid circulation in the Botrona quarry.

The hydraulic circuit of fluids in the case of Botrona quarry is very complex and it is here extremely simplified and referred to with the general term *reservoir*. In an ideal case, two hydraulic paths, both related to a same reservoir at some depth, should show the same level of horizontal diversion (Fig. 9a). Differently, OVA and DV veins formed at different fluid pressures, as testified by the different levels of horizontal diversion attained by the two systems (Fig. 3b).

Two possible scenarios can explain the occurrence of unconnected hydraulic paths in such close spatial association:

- Different hydraulic systems are related to distinct hydraulic circuits with reservoirs at different depths. The system related to the deepest reservoir (DV in the Botrona quarry) has the highest fluid pressure (Fig. 9b);
- Different hydraulic systems (OVA and DV in the Botrona quarry) are simultaneously active. At some time,

a temporary drop in fluid pressure in the principal system (OVA) determined the formation of veins sealed by calcite. The rising fluid pressure in the still active minor system (DV) determined the horizontal diversion of veins at lower levels than the sealed system (Fig. 9c).

The proposed cyclic increase in fluid pressure in different hydraulic paths may explain the close spatial association of vein systems with the same mineral infilling. A localised increase in the volume due to fluid injection into well-defined spatially associated paths may also generate a transient closure of fractures in the intervening space, thereby favouring the physical separation between the two hydraulic paths.

The OVA and DV systems represent build-up and release of overpressure inducing stress permutation (e.g. horizontal diversion of veins) occurring in different hydraulic paths. The peculiarity of the vein systems observed in the Botrona quarry mainly resides in that the local switch in the minimum principal stress occurs at different depths despite the close spatial association of the OVA and DV vein systems.

Acknowledgements

The statistical analysis of structural data has been performed by StereoWin 2002 by R. Allmendinger. Readings of the manuscript by G. Molli and G. Musumeci have been appreciated. G. Nortje and an anonymous reviewer are thanked for constructive comments and suggestions. The associate editor J. Hippert is thanked for editorial assistance.

References

André, A.-S., Sasse, J., Lespinasse, M., 2001. New approach for the quantification of paleostress magnitudes: application to the Soultz vein system (Rhine graben, France). Tectonophysics 336, 215–231.

Angelier, J., 1984. Tectonic analysis of fault slip data sets. J. Geophys. Res. 89, 5835–5848.

Baer, G., Beyth, M., Reches, Z., 1994. Dikes emplaced into fractured basement, Timma Igneous Complex. Israel. J. Geophys. Res. 99, 24039–24050.

Beeler, N.M., Simpson, R.W., Hickman, S.H., Lockner, D.A., 2000. Pore fluid pressure, apparent friction, and Coulomb failure. J. Geophys. Res. 105, 25533–25542.

Bertini, M., Centamore, E., Jacobacci, A., Nappi, G., 1969a. Foglio 127, Piombino, Carta Geologica d'Italia 1:100.000. Servizio Geologico d'Italia, Roma.

Bertini, M., Centamore, E., Jacobacci, A., Nappi, G., 1969b. Note Illustrative della Carta Geologica d'Italia Foglio 127, Piombino. Servizio Geologico d'Italia, Roma. pp.66.

Boccaletti, M., Elter, P., Guazzone, G., 1971. Plate tectonics models for the development of Western Alps and Northern Apennines. Nature 234, 108–111.

Bonnet, E., Bour, O., Odling, N., Main, I., Berkowitz, B., Davy, P., Cowie, P., 2001. Scaling of fracture systems in geological media. Rev. Geophys. 39, 347–383.

Bons, P.D., 2001. The formation of large quartz veins by rapid ascent of fluids in mobile hydrofractures. Tectonophysics 336, 1–17.

Bossio, A., Costantini, A., Lazzarotto, A., Liotta, D., Mazzanti, R., Mazzei, R., Salvatorini, G., Sandrelli, F., 1993. Rassegna delle conoscenze sulla stratigrafia del Neoautoctono Toscano. Memorie della Società Geologica Italiana 49, 17–98.

Bour, O., Davy, P., Darcel, C., Odling, N., 2002. A statistical scaling model for fracture network geometry, with validation on a multiscale mapping of a joint network (Hornelen Basin, Norway). J. Geophys. Res. 107, 2113, doi:10.1029/2001JB000176.

Brace, W.F., 1978. A note on permeability changes in geologic materials due to stress. Pure Appl. Geophys. 116, 627–633.

Burgassi, P.D., Decandia, F.A., Lazzarotto, A., 1983. Elementi di stratigrafia e paleogeografia nelle Colline Metallifere (Toscana) dal Trias al Quaternario. Memorie della Società Geologica Italiana 25, 27–50.

Byerlee, J.D., 1978. Friction of rocks. Pure Appl. Geophys. 116, 615–626.

Chiodini, G., Frondini, F., Cardellini, C., Parello, F., Peruzzi, L., 2000. Rate of diffuse carbon dioxide Earth degassing estimated from carbon balance of regional aquifers: the case central Apennine. Italy. J. Geophys. Res. 105, 8423–8434.

Chiodini, G., Cardellini, C., Amato, A., Boschi, E., Caliro, S., Frondini, F., Ventura, G., 2004. Carbon dioxide Earth degassing and seismogenesis in central and southern Italy. Geophys. Res. Lett. 31, L07615, doi:10.1029/2004GL0019480.

Cornamusini, G., Elter, F.M., Sandrelli, F., 2002. The Corsica-Sardinia Massif as source area for the early northern Apennines foredeep system: evidence from debris flows in the "Macigno Costiero" (Late Oligocene, Italy). Int. J. Earth Sci. 91, 280–290.

Cox, S.F., Knackstedt, M.A., Braun, J., 2001. Principle of structural control on permeability and fluid flow in hydrothermal system. In: Richards, J., Tosdal, R. (Eds.), Deformation, Fluid Flow and Ore Deposits. Rev. Econ. Geol. 14, pp. 1–24.

Darcel, C., Bour, O., Davy, P., de Dreuzy, J.R., 2003. Connectivity properties of two-dimensional fracture networks with stochastic fractal correlation. Water Resour. Res. 39, 1272, doi:10.1029/2002WR001628.

de Dreuzy, J.-R., Darcel, C., Davy, P., Bour, O., 2004. Influence of spatial correlation of fracture centers on the permeability of two-dimensional fracture networks following a power law length distribution. Water Resources Research 40, W01502, doi:10.1029/2003WR002260.

Elter, P., 1975. Introduction à la géologie de l'Apennin septentrional. Bulletin de la Société Géologique de France 7, 956–962.

Favalli, M., Pareschi, M.T., 2004. Digital elevation model construction from structured topographic data: the DEST algorithm. J. Geophys. Res. 109, F04004, doi:10.1029/2004JF000150.

Foxford, K.A., Nicholson, R., Polya, D.A., Hebblethwaite, R.P.B., 2000. Extensional failure and hydraulic valving at Minas da Panasqueira, Portugal: evidence from vein spatial distribution, displacements and geometries. J. Struct. Geol. 22, 1065–1086.

Gillespie, P.A., Johnston, J.D., Loriga, M.A., McCaffrey, K.J.W., Walsh, J.J., Watterson, J., 1999. Influence of layering on vein systematics in line samples. In: McCaffrey, K.J.W., Lonergan, L., Wilkinson, J.J. (Eds.), Fractures, Fluid Flow and Mineralization. Geological Society, London, Special Publications, vol. 155, pp. 35–56.

Gerecek, H., 2007. Poisson's ratio values for rocks. Int. J. Rock Mech. Min. Sci. 44, 1–13.

Goodman, R.E., 1980. Introduction to Rock Mechanics. Wiley, New York, 450 pp.

Gudmundsson, A., 1999. Fluid pressure and stress drop in fault zones. Geophys. Res. Lett. 26, 115–118.

Jaeger, J.C., Cook, N.G.W., 1969. Fundamentals of Rock Mechanics. Methuen, London, 513 pp.

Jolly, R.J.H., Sanderson, D.J., 1997. A Mohr circle construction for the opening of a pre-existing fracture. J. Struct. Geol. 19, 887–892.

Johnston, J.D., McCaffrey, K.J.W., 1996. Fractal geometries of vein systems and the variation of scaling relationships with mechanism. J. Struct. Geol. 18, 349–358.

Marinelli, G., Barberi, F., Cioni, R., 1993. Sollevamenti neogenici e intrusioni acide della Toscana e del Lazio settentrionale. Memorie della Società Geologica Italiana 49, 279–288.

Mazzarini, F., 2004. Volcanic vent self-similar clustering and crustal thickness in the northern Main Ethiopian Rift. Geophys. Res. Lett. 31, L04604, doi:10.1029/2003GL0018574.

Mazzarini, F., Corti, G., Musumeci, G., Innocenti, F., 2004. Tectonic control on laccolith emplacement in the northern Apennines fold-thrust belt: the Gavorrano intrusion (southern Tuscany, Italy). In: Breitkreuz, C., Petford, N. (Eds.), Physical Geology of High-level Magmatic Systems. Geological Society, London, Special Publications, vol. 234, pp. 151–161.

Miller, S.A., Collettini, C., Chiaraluce, L., Cocco, M., Barchi, M., Haus, B.J.P., 2004. Aftershock driven by high-pressure CO_2 at depth. Nature 427, 724–727.

Musumeci, G., Mazzarini, F., Corti, G., Barsella, M., Montanari, D., 2005. Magma emplacement in a ramp thrust anticline: The Gavorrano Granite (northern Apennines, Italy). Tectonics 24, TC6009, doi:10.1029/2005TC001801. TC6009.

Nicholson, R., Pollard, D.D., 1985. Dilation and linkage of echelon cracks. J. Struct. Geol. 7, 583–590.

Orife, T., Lisle, R.J., 2003. Numerical processing of palaeostress results. J. Struct. Geol. 25, 949–957.

Pollard, D.D., Segall, P., Delaney, P.T., 1982. Formation and interpretation of dilatant echelon cracks. Geol. Soc. Am. Bull. 93, 1291–1303.

Press, W.H., Flammery, B.P., Teukolsky, S.A., Vetterling, W.T., 1986. Numerical Recipes: The Art of Scientific Computing. Cambridge University Press, Cambridge, UK, 818 pp.

Roberts, S., Sanderson, D.J., Gumiel, P., 1999. Fractal analysis and percolation properties of veins. In: McCaffrey, K.J.W., Lonergan, L., Wilkinson, J.J. (Eds.), Fractures, Fluid Flow and Mineralization. Geological Society, London, Special Publications, vol. 155. 71–16.

Secor, D.T., 1965. Role of fluid pressure in jointing. Am. J. Sci. 263, 633–646.

Serri, G., Innocenti, F., Manetti, P., 2001. Magmatism from Mesozoic to Present: petrogenesis, time-space distribution and geodynamic implications. In: Vai, G.B., Marini, I.P. (Eds.), Anatomy of an Orogen: the Apennines and Adjacent Mediterranean Basin. Kluwer Academic Publishers, London, pp. 77–104.

Sibson, R.H., 2000. Fluid involvement in normal faulting. J. Geodyn. 29, 469–499.

Srivastava, D.C., Engelder, T., 1990. Crack-propagation sequence and pore fluid conditions during fault-bend folding in the Appalachian Valley and Ridge, central Pennsylvania. Geol. Soc. Am. Bull. 102, 116–128.

Suppe, J., 1985. Principles of Structural Geology. Prentice-Hall, Englewood Cliffs, NJ, 537 pp.

Turcotte, D.L., Schubert, G., 2002. In: Geodynamics, second ed. Cambridge University Press, Cambridge, UK, 456 pp.

Vermilye, J.M., Scholz, C.H., 1995. Relation between vein length and aperture. J. Struct. Geol. 17, 423–434.

Walsh, J.J., Watterson, J., 1993. Fractal analysis of fracture patterns using the standard box-counting technique: valid and invalid methodologies. J. Struct. Geol. 15, 1509–1512.